nature geoscience

Article

https://doi.org/10.1038/s41561-025-01700-9

Strong 2023–2024 El Niño generated by ocean dynamics

Received: 4 December 2024

Accepted: 10 April 2025

Published online: 23 May 2025

Check for updates

Qihua Peng [1] ✉, Shang-Ping Xie [1] ✉, Ayumu Miyamoto [1], Clara Deser [2], Pengcheng Zhang [1] & Matthew T. Luongo [1,3,4]

Globally, 2023 was the hottest year on record and saw the development of a strong El Niño with widespread impacts. This El Niño event was unusual for its strong oceanic warming yet muted Southern Oscillation and wind anomalies over the tropical Pacific. This discrepancy is perplexing given the historically close coupling of El Niño and the Southern Oscillation. Atmospheric model experiments show that warming in the Atlantic and Indian Oceans in 2023 and the slow background sea surface temperature trend reduced the surface wind response over the tropical Pacific by modulating the Walker circulation. We develop a hindcast system that reproduces 87% of the June–December El Niño warming even without wind stress feedback after April 2023. The intense oceanic warming was primarily driven by the strong build-up of western Pacific heat content during the preceding prolonged La Niña. This indicates that the 2023–2024 El Niño primarily arose from oceanic processes, independent of the classic positive Bjerknes feedback mechanism. Due to the strong ocean memory, this event was highly predictable at long time leads. Climate model simulations suggest that such 2023-like El Niños may become more frequent in a warming climate.

A prolonged three-year La Niña took place during 2020–2023 (refs. 1,2), building up record-breaking ocean heat content (OHC) in the tropical western Pacific (Extended Data Fig. 1f). This La Niña decayed around March 2023, followed by an extreme coastal El Niño off Peru during March–May (Extended Data Fig. 1a)[3]. From June onward, intense sea surface temperature (SST) warming was observed in the eastern equatorial Pacific Ocean (Figs. 1a and 2c and Extended Data Fig. 1), indicating the onset of a basin-scale El Niño. The SST warming signals then propagated westward from the eastern Pacific[4,5] (Fig. 2c). The eastern Pacific SST anomaly (SSTA) peaked during November–December, with the Niño 3 index exceeding +2 °C and then rapidly declined after December 2023, returning to normal levels around April 2024 (Fig. 2c). The average June–January (1) ('1' refers to the year following the peak El Niño) Niño 3 SSTA was +1.93 °C, making the 2023–2024 El Niño comparable in magnitude to the strong El Niños of 1982–1983, 1997–1998 and 2015–2016 (Fig. 1a,b,e,f). The central-eastern Pacific warming during this event was dominated by interannual variability (Extended Data Fig. 2d), contributing to record global temperatures two years in a row (2023–2024)[6]. The 2023–2024 El Niño caused worldwide environmental impacts, such as intense heatwaves in 2023[7], record drought and wildfires in the Amazon during 2023–2024 (ref. 8) and torrential rains in the southwestern United States in early 2024 (ref. 9).

During April and August 2023, the equatorial Pacific exhibited consistent positive sea level anomalies (SLA), followed by the development of a weak zonal dipole pattern during September to December (Fig. 2c). This behaviour contrasts with the pronounced zonal dipole patterns seen in other comparable El Niños (Figs. 1a,b and 2c,d,g–j). In 2023, the tropical North Atlantic (0–70° W, Equator–30° N) experienced record-breaking SSTAs exceeding 1.2 °C (Extended Data Fig. 2a,e)[5,10,11]. Typically, tropical Atlantic SSTAs are weak during the

[1]Scripps Institution of Oceanography, University of California San Diego, La Jolla, CA, USA. [2]National Center for Atmospheric Research, Boulder, CO, USA. [3]Cooperative Institute for Climate, Ocean, and Ecosystem Studies, University of Washington, Seattle, WA, USA. [4]School of Oceanography, University of Washington, Seattle, USA. ✉e-mail: q2peng@ucsd.edu; sxie@ucsd.edu

https://doi.org/10.1038/s41561-025-01700-9

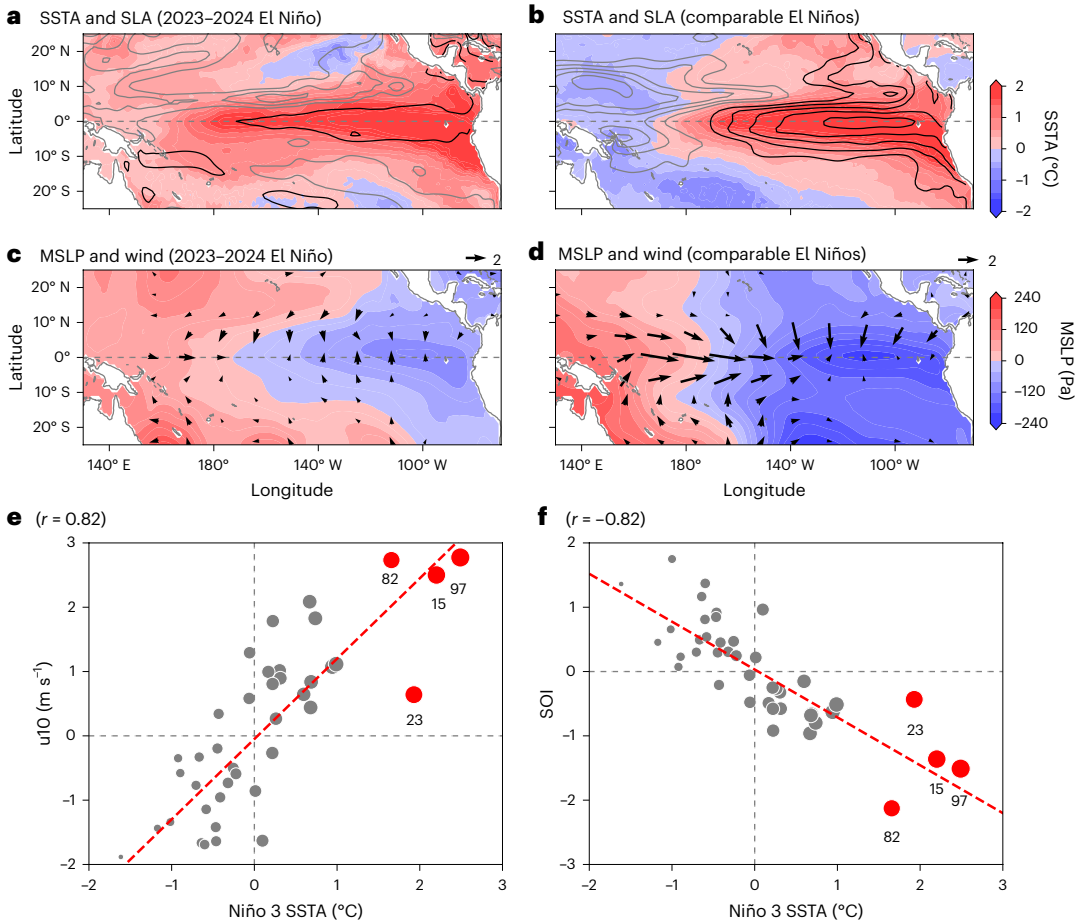

Fig. 1 | Climate states for the 2023–2024 El Niño. a,**b**, June–January (1) observed SSTA (°C, colour shading) and SLA (contours with an interval of 0.04 m; positive black and negative grey) for the 2023–2024 El Niño (**a**) and the other comparable El Niño composite (**b**). **c**,**d**, Same as **a**,**b** except for the mean sea level pressure (MSLP; colour shading) and 10-m wind anomalies (m s^{-1}, vectors). **e**,**f**, Scatter plot for June–January (1) Niño 3 averaged SSTAs (°C) versus concurrent CWP (140° E–160° W, 5° S–5° N) 10-m zonal wind anomalies (u10) (**e**) and SOI (**f**). The red labelled dots represent the four strong El Niños of 1982–1983, 1997–1998, 2015–2016 and 2023–2024. The dot size represents the amplitude of Niño 3 SSTAs.

development of an El Niño[12–14], making the strong concurrent warming of the eastern Pacific and tropical Atlantic during 2023–2024 highly unusual. Pronounced positive SSTAs were also observed in the tropical western Indian Ocean (40° E–70° E, 10° S–10° N), reaching a record-breaking value of +1.2 °C at the end of 2023 (Extended Data Fig. 2e). Tropical Indo-Atlantic warming is known to be unfavourable for El Niño development[12,15–18]. During August–November 2023, strong Indian Ocean Dipole (IOD) developed, with the dipole mode index reaching ~1.6 °C, the fourth strongest since 1980. Intense cooling in the eastern pole (warming in the western pole) during a positive IOD could induce westerly (or easterly) wind anomalies over the central Pacific, creating favourable (unfavourable) conditions for El Niño[19,20].

It is widely accepted that El Niño arises through positive air–sea feedback between surface wind perturbations and SSTAs[21]. Niño 3 warming is typically associated with westerly wind anomalies (or a negative Southern Oscillation Index, SOI), with a correlation of 0.82 (−0.82) (Fig. 1e,f). However, atmospheric anomalies during the strong 2023–2024 El Niño were mysteriously moderate (Fig. 1c)[11]. Specifically, there are sizeable westerly wind, sea level pressure (SLP) and rainfall anomalies near the equator during June 2023–January 2024, but the amplitude of these atmospheric anomalies is much smaller than expected from the composite of similar intensity El Niños (1982–1983, 1997–1998 and 2015–2016) (Figs. 1c,d and 2a,b). The central-western Pacific (CWP) zonal wind anomaly was only 27% of the expected value based on 1982–2023 regressions (Fig. 1e,f), varying between −14% and 57% depending on the time window (Extended Data Fig. 1g). Consistent with the weaker wind anomalies, the June 2023 to January 2024 averaged SLP difference between the eastern and western Pacific (or SOI) is only 31% of what is expected from the historical regression, varying between 13% and 57% across months (Extended Data Fig. 1g). The contrast between strong oceanic warming and muted surface wind or Southern Oscillation (SO) anomalies indicates that the Bjerknes feedback was not well established during this event. Important questions arise regarding the 2023–2024 El Niño: what drove the pronounced warming of the eastern equatorial Pacific given the central importance of the zonal wind (for example, Bjerknes) feedback for El Niño growth? What kept wind anomalies so moderate given that the SSTAs were so strong? Here we investigate these questions using global climate models of varied complexity, including a unique wind-stress-prescribed hindcast system. This system allows us to quantify the impacts of wind stress anomalies on the development of this El Niño. Our results show that the build-up of OHC anomalies in the western Pacific following the three-year La Niña triggered the 2023–2024 El Niño, whereas wind stress anomalies and Bjerknes feedback played a secondary role in the development of this event. These results represent a conceptual advance in understanding El Niño/Southern Oscillation (ENSO) dynamics: El Niño does not necessarily develop through positive air–sea interactions. Even without the Bjerknes feedback (or the SO component), ocean dynamics alone can generate a strong El Niño.

https://doi.org/10.1038/s41561-025-01700-9

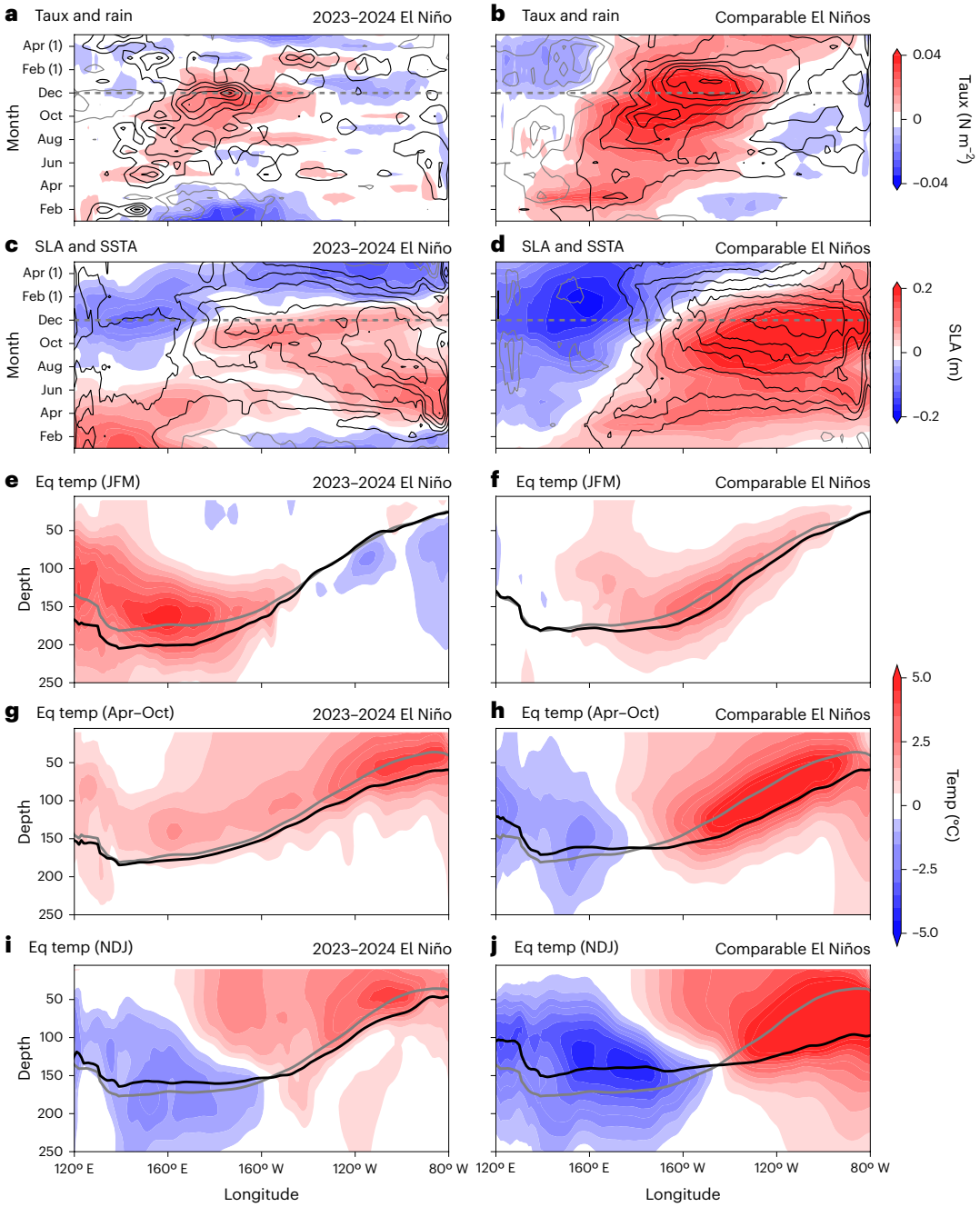

Fig. 2 | Evolution of the 2023–2024 El Niño and the composite El Niño based on comparable events in 1982–1983, 1997–1998 and 2015–2016. a,**c**, Hovmöller diagram of equatorial zonal wind stress (Taux; colour shading; N m^{-2}) and rainfall anomalies (contours with an interval of 1.5 mm per day; positive black and negative grey; amplitude smaller than 3 mm per day omitted) (**a**) and SLA (m, colour shading) and SSTA (°C, contours with an interval of 0.5 °C; positive black and negative grey) (**c**) for the 2023–2024 El Niño. **e**,**g**,**i**, The January–March (JFM) (**e**), April–October (**g**) and November–January (1) (NDJ) (**i**) averaged equatorial ocean temperature anomalies (Eq temp; °C, colour shading) for the 2023–2024 El Niño. The black (grey) line represents the 2023 (climatological) 20 °C isotherm. **b**,**d**,**f**,**h**,**j**, Similar to the left panels but for the El Niño composite based on comparable events. All anomalies are meridionally averaged over 2° S–2° N.

Inter-basin impacts

To investigate the mechanisms moderating the surface wind response during the 2023–2024 El Niño, we performed five Atmospheric General Circulation Model (AGCM) experiments (Methods and Extended Data Table 1). Forced by observed global SSTs, the control run (aCTRL) captures the overall observed atmospheric anomalies over the tropical Pacific, including the weaker atmospheric responses during the 2023–2024 event relative to other comparable El Niños, the easterly anomalies at the beginning of 2023 and the sustained westerly anomalies from June to December (Supplementary Fig. 1a,b). This underscores the utility of the AGCM in exploring the primary physical mechanisms behind the weak atmospheric response to the 2023 El Niño event.

In 2023, the North Atlantic and western Indian Oceans experienced record-breaking warming (Extended Data Fig. 2a,e), which could potentially affect atmospheric anomalies over the tropical Pacific Ocean[15–18,22]. To explore this possibility, we conducted three AGCM experiments forced by (1) Pacific detrended SSTAs (aPac), (2) Indian–Atlantic detrended SSTAs (aIndAtl) and (3) the background SST trends for 1982–2023 (aTrend) (Extended Data Fig. 2a–c). This approach allowed us to assess the impacts of Pacific and Indian–Atlantic

https://doi.org/10.1038/s41561-025-01700-9

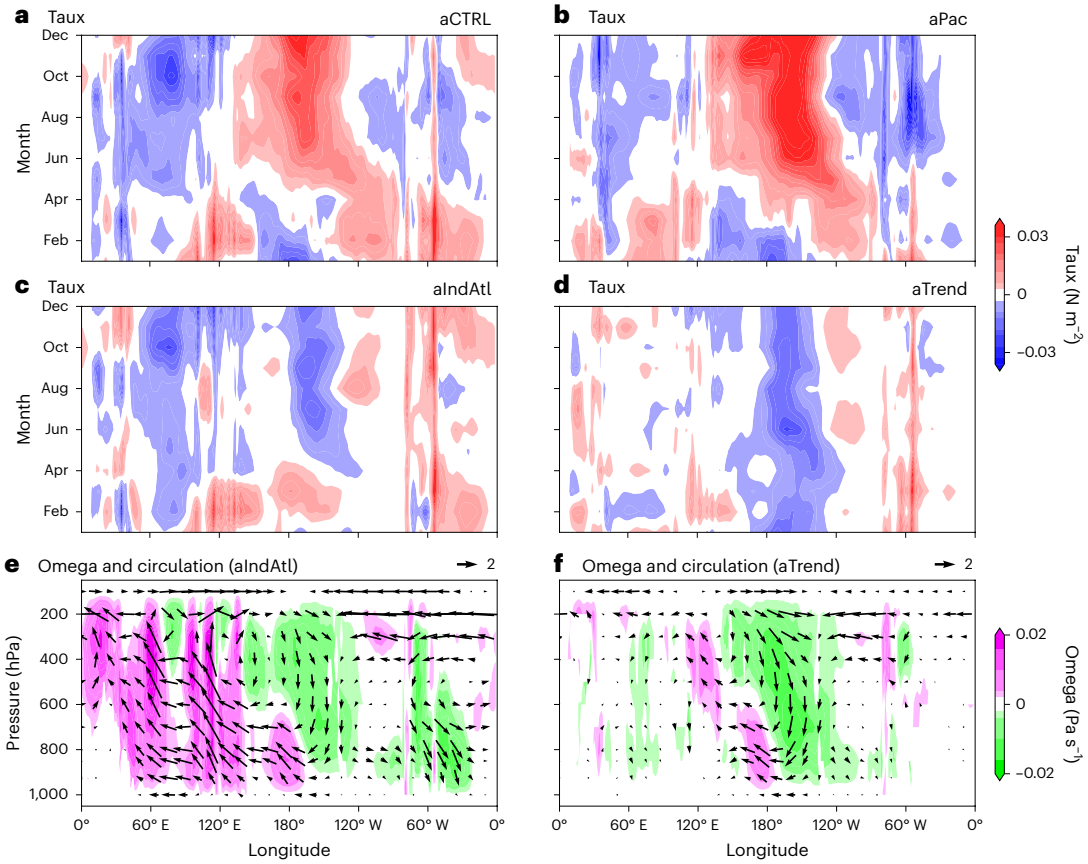

Fig. 3 | Atmospheric response from the AGCM experiments. a–**d**, Hovmöller diagram of equatorial zonal wind stress anomalies (colour shading; N m^{-2}) from aCTRL (**a**), aPac (**b**), aIndAtl (**c**) and aTrend (**d**) runs (Methods). **e**,**f**, The associated June–December averaged vertical velocity (Pa s^{-1}, colour shading; a positive value indicates ascending motions) and Walker circulation changes (vectors, m s^{-1}; the vertical velocity is magnified by a factor of 200 for visualization purposes) from aIndAtl (**e**) and aTrend (**f**).

detrended SSTAs and global SST trends, respectively (Methods). Figure 3b shows that the westerly wind stress anomalies are nearly twice as large in aPac as in aCTRL during the El Niño developing phase, indicating that the Pacific detrended SSTAs could drive large surface wind responses in 2023. Importantly, the aIndAtl results indicate that inter-basin impacts from the Atlantic and Indian oceans induce easterly wind stress anomalies (0.16 N m^{-2}) over the central Pacific (150° W–170° W, 2° S–2° N), with high consistency across model members (Supplementary Fig. 1c). This leads to a 34% reduction in the surface wind response to El Niño during July–December, broadly consistent with previous studies that strong warming in the tropical Atlantic and Indian oceans forces a Matsuno–Gill response[23] with an anomalous Walker circulation sinking branch and easterly surface wind anomalies over the tropical eastern Pacific (Fig. 3e)[12,15–18,22,24,25]. Recent studies employing distinct methodologies have confirmed the importance of pantropical forcing in reducing atmospheric responses during this event[5,11,26].

The long-term SST trend over 1982–2023 played a comparable role in reducing the atmospheric response through modulating the Walker circulation (Fig. 3d,f). The SST trend is characterized by relatively large warming in the Indian, Atlantic and western Pacific oceans but muted warming in the eastern tropical Pacific (Extended Data Fig. 2c). The strong warming trend in the Indian and Atlantic oceans induces easterly wind anomalies over the central Pacific through the Matsuno–Gill response[16,24]. In addition, the enhanced zonal SST gradient in the Pacific Ocean accelerates the Walker circulation[27,28]. Together, these processes result in easterly wind anomalies near the dateline with high inter-member consistency (Supplementary Fig. 1c). From a different perspective, the slower warming trend in the tropical eastern Pacific compared to the overall tropical mean results in slightly negative relative SST trends[29] (Supplementary Fig. 2a), reducing local convection[29–31] and trade wind responses in this region (Methods and Supplementary Fig. 2b–d).

Oceanic dynamics

To reveal the key physical mechanism for the strong oceanic warming of the 2023–2024 El Niño, we conduct a mixed layer heat budget analysis based on reanalysis data (Methods). Extended Data Fig. 3a shows that vertical advection drives the Niño 3 SST warming during June–December. The vertical advection term is dominated by the thermocline feedback (TH) term (Methods and Extended Data Fig. 3b). Specifically, large subsurface warming was observed in the equatorial Pacific during June–December 2023 (Extended Data Fig. 4c–e), which the mean upwelling pumps into the mixed layer, raising SST there. Additionally, the reduced upwelling due to the weakened trade winds contributes to the SST warming through Ekman feedback (EK) (Methods and Extended Data Fig. 3b).

Oceanic general circulation models (OGCMs) have been widely used to simulate and investigate SST variability[32,33]. Whereas observed air temperature and specific humidity are often prescribed in calculating surface heat flux, the implied atmospheric thermodynamic forcing of the ocean is physically flawed because these quantities can also be a result of the SSTA and such simulations fail to capture air–sea interactions at the interface[34,35]. Thus, the results of such OGCM experiments might be misleading, especially if SST is the primary focus[35]. Here we adopt an advanced approach to overcoming this issue by forcing a

coupled GCM (CGCM) with observed wind stress, while otherwise retaining the model's ocean–atmosphere coupling (Methods). We conducted sensitivity experiments to investigate the detailed physical processes underlying the 2023–2024 event (Methods and Extended Data Table 2). The control run (CTRL) is forced with observed daily wind stress. Figure 4a shows that the CTRL run successfully reproduces the observed El Niño/La Niña events, with a high correlation of 0.90 between the simulated and observed Niño 3 SST variability. The standard error is 0.14 °C, a remarkable achievement enabled by realistic thermodynamic coupling in our 'wind stress overriding' CTRL simulation. Extended Data Fig. 4 further shows that the simulated SSTA, SLA and equatorial subsurface temperature anomalies for the 2023–2024 El Niño agree with observations remarkably well. The good model–observation agreement gives us confidence in using this powerful protocol to uncover the key factors for the 2023–2024 El Niño.

Restarting from the initial condition obtained from the CTRL run on 1 April 2023, the InitApr2023 run prescribes observed wind stress but excludes the 31-day running-mean wind stress anomalies from that date onward. High-frequency weather variations are retained to minimize model bias[36], but whether these high-frequency signals are included or not turns out not to affect the conclusions of our study (Methods and Supplementary Fig. 3). The solutions thus isolate the impacts of the initial conditions on the 2023–2024 strong El Niño. The difference, CTRL-InitApr2023 (termed Wind2023), represents the influence of subsequent wind stress anomalies. Figure 4b shows that the initial conditions on 1 April 2023 play a dominant role in the 2023–2024 El Niño event, accounting for 87% of the Niño 3 SST increase averaged in June–December. In contrast, concurrent wind stress anomalies—typically considered crucial for El Niño development—contribute only 13% of the SST warming, with their influence primarily confined to the end of the year, consistent with the emergence of westerly wind anomalies during that period (Fig. 2a). For comparison, we conducted similar experiments (InitAprOther) initialized on 1 April for the other three comparable El Niños of 1982–1983, 1997–1998 and 2015–2016 (Methods). Figure 4c shows that wind stress anomalies (WindOther) contribute nearly all of the Niño 3 SST warming after August. This result aligns with widely accepted ENSO theory[21,37] and stands in stark contrast to the results for the 2023–2024 El Niño.

The initial condition for the 2023–2024 El Niño is characterized by extraordinarily large positive OHC anomalies (or equivalently SLAs) in the western Pacific (Fig. 4d) from 20° N to 30° S. Indeed, the upper-300-m OHC anomaly in the western Pacific at the beginning of 2023 reached its highest value (2.43×10^{22} J) since 1982 (Extended Data Fig. 1f). The large positive OHC anomalies followed a three-year La Niña, persisting in the western Pacific since June 2020 (Extended Data Fig. 5a,d–f). Extended Data Fig. 5 shows that the intensified trade winds during 2020–2022 contributed to the build-up of OHC in the western Pacific Ocean (WPAC) through Ekman convergence and downwelling Rossby waves. The strongly tilted thermocline in the east–west direction was balanced by the enhanced easterly trade winds. During March–April 2023, the equatorial trade winds returned to normal as the La Niña decayed (as mimicked by InitApr2023) (Extended Data Fig. 5c,h), disrupting the balance between the zonal thermocline gradient and the trade winds and causing the accumulated warm water (or SLAs) in the western Pacific to propagate eastward along the equator as downwelling Kelvin waves (Fig. 4f, Extended Data Fig. 5g–i and left panels of Extended Data Fig. 6). In the eastern Pacific, SST increased as the mean upwelling transported the subsurface warming into the mixed layer (Extended Data Fig. 7a–d), consistent with the heat budget results shown above (Extended Data Fig. 3b).

In comparison, a major El Niño is typically preceded by a deepened thermocline in the central equatorial Pacific (Figs. 2f and 4e) in a process known as the 'thermocline recharge'[38,39]. The InitAprOther experiment shows that without the wind stress feedback, the recharged thermocline depth anomalies disperse quickly (Fig. 4g and right panels of Extended Data Fig. 6) and the equatorial Pacific Ocean returns to normal in three months (Extended Data Fig. 7e–h). In these comparable El Niño events, the westerly wind anomalies predominantly drive the sustained eastern Pacific warming as part of a marked east–west dipole in subsurface temperature along the mean thermocline as required by the zonal momentum balance (Fig. 4i,k). Unlike this tilt-mode adjustment, subsurface anomalies remained positive across the equatorial Pacific for most of 2023 (Figs. 2g and 4j), characteristic of Kelvin waves that deepen the thermocline. The build-up of OHC in the western Pacific before April 2023 that slowly fed the deepened thermocline in the equatorial Pacific (Fig. 4d,f) is an interesting topic for further research.

The slow ocean dynamic adjustments imply that the 2023–2024 El Niño can be predicted at long leads, as OHC carries memory and serves as the major source of predictability[26,40]. Indeed, recent studies noted skilful predictions of the 2023–2024 event[26,40–42], but the underlying physical processes and the unique air–sea characteristics of this El Niño have not previously been fully explored through diagnostic analysis and insightful model experiments as done here. Supplementary Fig. 4 presents the forecasts in the North American Multi-Model Ensemble. With large OHC stored in the western Pacific following the three-year La Niña, most models predicted the El Niño at the beginning of 2023. When initialized on 1 April 2023, the predicted Niño 3.4 (Niño 3) SSTA for December 2023 was 1.64 °C (1.73 °C), closely matching observations (Supplementary Fig. 4).

Insights into ENSO dynamics

Statistical analysis of historical events has led to important advances in understanding the coupled dynamics of El Niño and its flavours[43–46]. Our observational analysis has shown that the 2023–2024 El Niño was peculiar: the atmospheric responses to the strong equatorial Pacific SSTA were weak compared to those inferred from historical events. This suggests that the Bjerknes feedback was not fully established to promote the growth of this strong El Niño, a surprising result against widely accepted ENSO theory that centres on this coupled feedback mechanism[21,47]. Through advanced GCM experiments, we show that even in the absence of tropical air–sea feedbacks (or the SO component), ocean dynamics alone can generate a strong El Niño.

Our AGCM results reveal that strong tropical inter-basin impacts played a vital role in reducing the atmospheric anomalies over the tropical Pacific Ocean during 2023. Specifically, both the record-breaking warmth of the tropical Atlantic and western Indian oceans in 2023 and the tropical long-term SST trends induced anomalous Walker circulation subsidence and easterly surface wind anomalies over the central and eastern Pacific. These influences moderated the tropical atmospheric perturbations associated with the developing El Niño, preventing the full establishment of the Bjerknes feedback during this event. The 2023–2024 El Niño illustrates that ENSO is not a phenomenon confined to the tropical Pacific basin (Fig. 3) but can be strongly modulated by SST conditions in other tropical basins. This raises an important question of whether a single El Niño index (for example, Niño 3.4 SST) is a good measure of global atmospheric anomalies[29] (for example, the SO). The bottom panels of Fig. 1 show that the answer is yes for a statistically average/typical ENSO event, but individual events require a close look as we did here for the 2023–2024 El Niño.

We have developed an improved ocean hindcast system by forcing the ocean component in a CGCM with observed wind stress. This enables us to uncover the key physical processes underlying the strong oceanic warming despite weak Bjerknes feedback during this El Niño. We show that the unprecedented build-up of OHC (SLA) in the tropical western Pacific Ocean following a long-lasting La Nina drives SST warming in the eastern equatorial Pacific through downwelling Kelvin waves. As the trade winds returned to their climatological values with the decaying La Niña, downwelling Kelvin waves induced large subsurface warming in the eastern equatorial Pacific Ocean and raised SST through thermocline feedback. Wind stress anomalies, which

https://doi.org/10.1038/s41561-025-01700-9

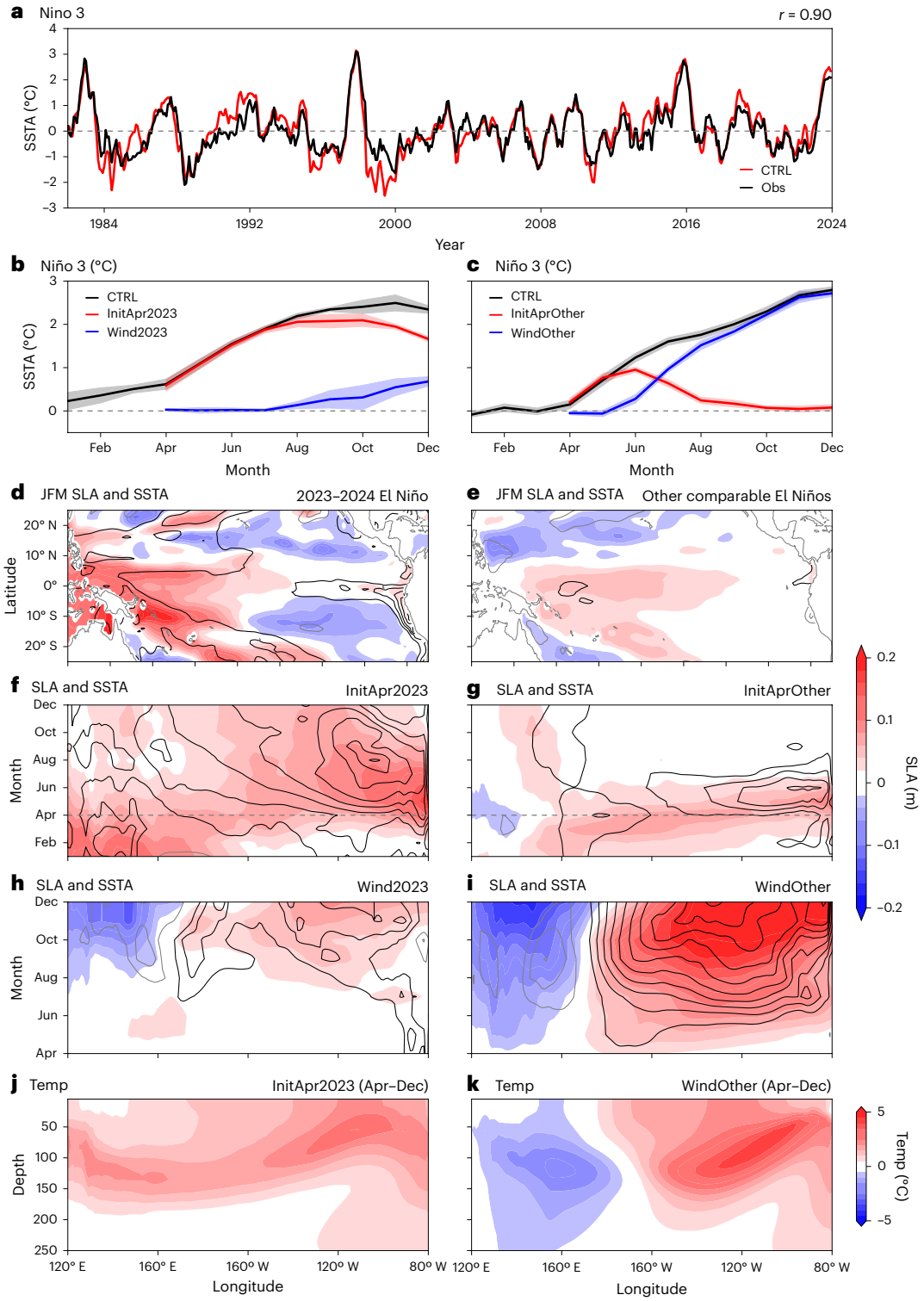

Fig. 4 | The impacts of ocean initial conditions and wind stress anomalies on the 2023–2024 El Niño and the other three comparable El Niños. a, Simulated (CTRL) and observed (Obs) Niño 3 SSTA (°C) during January1982–December 2023. **b**, Simulated Niño 3 SSTAs from the CTRL, InitApr2023 and their difference (Wind2023). **c**, Similar to **b** but for the composite of the other comparable El Niños. The solid lines in **b** and **c** indicate ensemble mean, and the error bands represent one inter-member standard deviation above and below the ensemble mean. **d**, Horizontal distribution of SLA (m, colour shading) and SSTA (°C, contours) averaged in JFM 2023 from the CTRL run, which generally represents the initial conditions for InitApr2023. **f**,**h**, Hovmöller diagram of equatorial SLA (m, colour shading) and SSTA (contours) from the InitApr2023 (**f**) and Wind2023 (**h**) experiment. Contours are shown at 0.5 °C intervals, with positive black and negative grey. **e**,**g**,**i**, Similar to **d**,**f**,**h** but for the composite of the other comparable El Niños (Methods). **j**,**k**, Longitude–depth diagram of April–December equatorial ocean temperature anomalies (°C, colour shading) from InitApr2023 (**j**) and WindOther (**k**), respectively.

have been widely considered essential in El Niño dynamics, played a secondary role in the development of the 2023–2024 event. Due to the memory of large OHC anomalies in WPAC, the North American Multi-Model Ensemble consistently predicted a Niño 3.4 warming of ~1 °C as early as January–March 2023 (Supplementary Fig. 4) across the so-called spring predictability barrier.

Climate models project that the occurrences of 2023-like El Niño increase markedly in a future warmer climate, primarily due to more frequent strong positive SLA events in the western Pacific (Extended Data Fig. 8e,f and Methods). These stronger SLAs result from a more pronounced sea level response to wind stress (Extended Data Fig. 8g,h and Methods), potentially linked to factors such as reduced wave damping due to faster phase speeds from enhanced vertical stratification[48] or the nonlinear thermal expansion of seawater[49]. Further research is required to better understand the underlying physical processes.

Online content

Any methods, additional references, Nature Portfolio reporting summaries, source data, extended data, supplementary information, acknowledgements, peer review information; details of author contributions and competing interests; and statements of data and code availability are available at https://doi.org/10.1038/s41561-025-01700-9.

References

1. Hasan, N. A., Chikamoto, Y. & McPhaden, M. J. The influence of tropical basin interactions on the 2020–2022 double-dip La Niña. *Front. Clim.* **4**, 1001174 (2022).
2. Iwakiri, T. et al. Triple-dip La Niña in 2020–23: North Pacific atmosphere drives 2nd year La Niña. *Geophys. Res. Lett.* **50**, e2023GL105763 (2023).
3. Peng, Q., Xie, S.-P., Passalacqua, G. A., Miyamoto, A. & Deser, C. The 2023 extreme coastal El Niño: atmospheric and air-sea coupling mechanisms. *Sci. Adv.* **10**, eadk8646 (2024).
4. Geng, X., Kug, J.-S., Shin, N.-Y., Zhang, W. & Chen, H.-C. On the spatial double peak of the 2023–2024 El Niño event. *Commun. Earth Environ.* **5**, 691 (2024).
5. Hu, R. et al. Predicting the 2023/24 El Niño from a multi-scale and global perspective. *Commun. Earth Environ.* **5**, 675 (2024).
6. Xie, S.-P. et al. What made 2023 and 2024 the hottest years in a row? *npj Clim. Atmos. Sci.* **8**, 117 (2025).
7. Jiang, N. et al. Enhanced risk of record-breaking regional temperatures during the 2023–24 El Niño. *Sci. Rep.* **14**, 2521 (2024).
8. Espinoza, J.-C. et al. The new record of drought and warmth in the Amazon in 2023 related to regional and global climatic features. *Sci. Rep.* **14**, 8107 (2024).
9. L'Heureux, M. L. et al. How well do seasonal climate anomalies match expected El Niño–Southern Oscillation (ENSO) impacts? *Bull. Am. Meteorol. Soc.* **105**, E1542–E1551 (2024).
10. Zhao, J. et al. Lapsed El Niño impact on Atlantic and Northwest Pacific tropical cyclone activity in 2023. *Nat. Commun.* **15**, 6706 (2024).
11. Hong, C. C., Sullivan, A. & Chang, C. C. Impact of North Atlantic tripole and extratropical North Pacific extreme SSTs on the 2023/24 El Niño. *Geophys. Res. Lett.* **51**, e2024GL110639 (2024).
12. Cai, W. et al. Pantropical climate interactions. *Science* **363**, eaav4236 (2019).
13. Chang, P., Fang, Y., Saravanan, R., Ji, L. & Seidel, H. The cause of the fragile relationship between the Pacific El Niño and the Atlantic Niño. *Nature* **443**, 324–328 (2006).
14. Latif, M. & Grötzner, A. The equatorial Atlantic oscillation and its response to ENSO. *Clim. Dyn.* **16**, 213–218 (2000).
15. Ding, H., Keenlyside, N. S. & Latif, M. Impact of the equatorial Atlantic on the El Niño Southern Oscillation. *Clim. Dyn.* **38**, 1965–1972 (2012).
16. Wang, C. Three-ocean interactions and climate variability: a review and perspective. *Clim. Dyn.* **53**, 5119–5136 (2019).
17. Wang, J.-Z. & Wang, C. Joint boost to super El Niño from the Indian and Atlantic oceans. *J. Clim.* **34**, 4937–4954 (2021).
18. Yu, J.-Y. et al. Linking emergence of the central Pacific El Niño to the Atlantic multidecadal oscillation. *J. Clim.* **28**, 651–662 (2015).
19. Hameed, S. N., Jin, D. & Thilakan, V. A model for super El Niños. *Nat. Commun.* **9**, 2528 (2018).
20. Wu, J. et al. Boosting effect of strong western pole of the Indian Ocean dipole on the decay of El Niño events. *npj Clim. Atmos. Sci.* **7**, 6 (2024).
21. Bjerknes, J. Atmospheric teleconnections from the equatorial Pacific. *Mon. Weather Rev.* **97**, 163–172 (1969).
22. Kug, J.-S. & Kang, I.-S. Interactive feedback between ENSO and the Indian Ocean. *J. Clim.* **19**, 1784–1801 (2006).
23. Gill, A. E. Some simple solutions for heat-induced tropical circulation. *Q. J. R. Meteorol. Soc.* **106**, 447–462 (1980).
24. Li, X., Xie, S.-P., Gille, S. T. & Yoo, C. Atlantic-induced pan-tropical climate change over the past three decades. *Nat. Clim. Change* **6**, 275–279 (2016).
25. Wang, L., Yu, J.-Y. & Paek, H. Enhanced biennial variability in the Pacific due to Atlantic capacitor effect. *Nat. Commun.* **8**, 14887 (2017).
26. Zhao, S. et al. Explainable El Niño predictability from climate mode interactions. *Nature* **630**, 891–898 (2024).
27. Toda, M., Kosaka, Y., Miyamoto, A. & Watanabe, M. Walker circulation strengthening driven by sea surface temperature changes outside the tropics. *Nat. Geosci.* **17**, 858–865 (2024).
28. Watanabe, M. et al. Possible shift in controls of the tropical Pacific surface warming pattern. *Nature* **630**, 315–324 (2024).
29. L'Heureux, M. L. et al. A relative sea surface temperature index for classifying ENSO events in a changing climate. *J. Clim.* **37**, 1197–1211 (2024).
30. Johnson, N. C. & Xie, S.-P. Changes in the sea surface temperature threshold for tropical convection. *Nat. Geosci.* **3**, 842–845 (2010).
31. Van Oldenborgh, G. J. et al. Defining El Niño indices in a warming climate. *Environ. Res. Lett.* **16**, 044003 (2021).
32. Peng, Q. et al. Eastern Pacific wind effect on the evolution of El Niño: implications for ENSO diversity. *J. Clim.* **33**, 3197–3212 (2020).
33. Vecchi, G. A. & Harrison, D. The termination of the 1997–98 El Niño. Part I: mechanisms of oceanic change. *J. Clim.* **19**, 2633–2646 (2006).
34. Deremble, B., Wienders, N. & Dewar, W. CheapAML: a simple, atmospheric boundary layer model for use in ocean-only model calculations. *Mon. Weather Rev.* **141**, 809–821 (2013).
35. Seager, R., Blumenthal, M. B. & Kushnir, Y. An advective atmospheric mixed layer model for ocean modeling purposes: global simulation of surface heat fluxes. *J. Clim.* **8**, 1951–1964 (1995).
36. Luongo, M. T., Brizuela, N. G., Eisenman, I. & Xie, S. P. Retaining short-term variability reduces mean state biases in wind stress overriding simulations. *J. Adv. Model. Earth Syst.* **16**, e2023MS003665 (2024).
37. Hu, S. & Fedorov, A. V. The extreme El Niño of 2015–2016: the role of westerly and easterly wind bursts, and preconditioning by the failed 2014 event. *Clim. Dyn.* **52**, 7339–7357 (2019).
38. Jin, F.-F. An equatorial ocean recharge paradigm for ENSO. Part I: conceptual model. *J. Atmos. Sci.* **54**, 811–829 (1997).
39. Meinen, C. S. & McPhaden, M. J. Observations of warm water volume changes in the equatorial Pacific and their relationship to El Niño and La Niña. *J. Clim.* **13**, 3551–3559 (2000).
40. Lian, T., Wang, J., Chen, D., Liu, T. & Wang, D. A strong 2023/24 El Niño is staged by tropical Pacific Ocean heat content buildup. *Ocean-Land-Atmos. Res.* **2**, 0011 (2023).

41. Petrova, D., Rodó, X., Koopman, S. J., Tzanov, V. & Cvijanovic, I. The 2023/24 El Niño and the feasibility of long-lead ENSO forecasting. *Bull. Am. Meteorol. Soc.* **105**, E1915–E1928 (2024).
42. Zhang, R.-H., Zhou, L., Gao, C. & Tao, L. Real-time predictions of the 2023–2024 climate conditions in the tropical Pacific using a purely data-driven transformer model. *Sci. China Earth Sci.* **67**, 3709–3726 (2024).
43. Ashok, K., Behera, S. K., Rao, S. A., Weng, H. & Yamagata, T. El Niño Modoki and its possible teleconnection. *J. Geophys. Res. Oceans.* **112**, C11007 (2007).
44. Kao, H.-Y. & Yu, J.-Y. Contrasting eastern-Pacific and central-Pacific types of ENSO. *J. Clim.* **22**, 615–632 (2009).
45. Kug, J.-S., Jin, F.-F. & An, S.-I. Two types of El Niño events: cold tongue El Niño and warm pool El Niño. *J. Clim.* **22**, 1499–1515 (2009).
46. Takahashi, K., Montecinos, A., Goubanova, K. & Dewitte, B. ENSO regimes: reinterpreting the canonical and Modoki El Niño. *Geophys. Res. Lett.* **38**, L10704 (2011).
47. Wyrtki, K. El Niño—the dynamic response of the equatorial Pacific Oceanto atmospheric forcing. *J. Phys. Oceanogr.* **5**, 572–584 (1975).
48. Zheng, X.-T., Hui, C., Han, Z.-W. & Wu, Y. Advanced peak phase of ENSO under global warming. *J. Clim.* **37**, 5271–5289 (2024).
49. Widlansky, M. J., Long, X. & Schloesser, F. Increase in sea level variability with ocean warming associated with the nonlinear thermal expansion of seawater. *Commun. Earth Environ.* **1**, 9 (2020).

Methods

Observational datasets and large-ensemble simulation

We used the monthly National Oceanic and Atmospheric Administration (NOAA) Optimum Interpolation Sea Surface Temperature version 2 dataset (OISSTv2) during 1982–2024 (ref. 50) and the Global Precipitation Climatology Project (GPCP) during 1979–2024 (ref. 51). The ocean temperature, mixed layer depth, currents and monthly sea level spanning 1980–2024 are obtained from the National Centers for Environmental Prediction (NCEP) Global Ocean Data Assimilation System (GODAS). The daily and monthly surface wind, total rainfall and air–sea fluxes during 1940–2024 are derived from the ERA5 reanalysis data[52]. All the anomalies in this study are defined relative to the 1982–2022 climatological value.

We analyse outputs from the 99-member CESM-LENS2 to investigate projected changes in the frequency of 2023-like El Niños. Each member differs slightly from others in the initial air temperature field and is driven by historical greenhouse gas and aerosol forcings from 1850 to 2014, followed by the Shared Socioeconomic Pathway 7.0 (SSP3–7.0) emissions scenario from 2015 to 2100. To investigate future ENSO changes, we filtered out low-frequency signals with periods longer than ten years for all variables used. We define 2023-like events as those with a WPAC SLA greater than 4.5 cm in JFM and a Niño 3 SSTA above 0.5 °C in November–January (1) (NDJ). Extended Data Fig. 8a,b shows that El Niño events defined this way share similar characteristics with the 2023–2024 event, including large western Pacific SLAs during the onset stage, eastward (westward) propagation of SLAs (SSTAs) together with weak equatorial zonal wind stress anomalies during the developing phase. Additionally, the simulated other non-2023-like El Niños (other El Niños excluding 2023-like events) are characterized by weak SLAs in the central Pacific during the onset and strong east–west tilted SLAs with intense westerly wind anomalies during the developing and peak phases, resembling the observed El Niños of 1982–1983, 1997–1998 and 2015–2016 (Extended Data Fig. 8c,d). We track the occurrences of the 2023-like events during 1900–1990 and 2000–2090 to represent the present and future climates, respectively.

AGCM experiments

We use the Community Atmosphere Model version 6 (CAM6) to explore the mechanism underlying the muted atmospheric response to the 2023–2024 El Niño. The model resolution is 0.9° latitude × 1.25° longitude ('f09_f09') with 32 sigma levels in the vertical. We performed five experiments, each comprising ten ensemble members with slightly different initial conditions. In the aCTRL run, we force CAM6 with observed monthly OISST from January 1982 to December 2023. The aCTRL is radiatively forced by historical forcing until 2014 and then subsequently by the Coupled Model Intercomparison Project phase 6 (CMIP6) SSP3–7.0 scenario[53].

Restarting from the initial state from aCTRL on January 2023, we performed two sensitivity experiments forced with the detrended 2023 SSTAs (Extended Data Fig. 2b and Extended Data Table 1) regionally in the Pacific Ocean (aPac; with 5° linear tapering zones outside this region) and the Indian–Atlantic Ocean (aIndAtl) while employing climatological SST during 1982–2022 in other regions. The solution of aPac (aIndAtl) thus isolates the atmospheric response to Pacific (Indian–Atlantic) Ocean regional SSTAs in 2023. Additionally, a third sensitivity experiment, aTrend, was conducted by forcing the model with the global long-term trend component of SSTAs in 2023 (Extended Data Fig. 2c) to assess atmospheric responses to SST trends. The slower warming trend in the tropical eastern Pacific, compared to the overall tropical mean, results in a slightly negative relative SST trend in that region[29]. Because of the weak horizontal temperature gradient in the tropical troposphere, relative SST is a good measure of local atmospheric instability[29–31], exploring the impacts of Pacific relative SST in 2023–2024 could offer valuable insights into the physical processes underlying the weak atmospheric response. We thus ran an additional experiment (aPac_RSST), forcing the AGCM with relative SSTAs in the Pacific, while using climatological SSTs in other areas. Supplementary Fig. 2b–d shows that atmospheric responses in aPac_RSST are weaker compared to aPac. Indeed, a negative relative SST trend indicates that the same level of warming in the eastern Pacific in 2023 triggers weaker convective anomalies compared to the 1982–2022 mean state, thereby reducing trade wind and SO responses.

Mechanisms for long-term trends and interannual anomalies of SST are distinct, the former due to radiative forcing and/or multidecadal variability while the latter due to coupled modes organized in ocean basins (for example, ENSO and IOD). This justifies our AGCM experiments that isolate interannual SST anomalies of the Pacific from those of the Indo-Atlantic basins (Fig. 3). It is important to note that the SST trends are to first order spatially uniform from the Atlantic to the western Pacific (Extended Data Fig. 2c), consistent with greenhouse radiative forcing. The artificial division of SST trends into geographical ocean basins introduces spurious gradients, resulting in spurious wind responses that mutually offset each other over the western Pacific. We thus did not perform additional sensitivity experiments with basin-specific SST trends.

Wind-stress-prescribed CGCM experiments

We used the Geophysical Fluid Dynamics Laboratory coupled model version 2.1 (ref. 54) to reveal the detailed physical processes underlying the strong oceanic warming for the 2023–2024 El Niño. The ocean component is based on the Modular Ocean Model code (MOM4). The ocean model resolution is 1° in latitude and longitude, with a finer meridional resolution of 1/3° near the equator. There are 50 vertical levels, with layer thickness gradually increasing from 10 m near the surface to about 366 m in the deep ocean. The atmosphere and land components are referred to as AM2.1 and LM2.1, with a horizontal resolution of 2° latitude × 2.5° longitude; the atmospheric model has 24 levels in the vertical. The model is forced by the historical radiative forcing of CMIP5 for 1941–2005 and representative concentration pathway 4.5 thereafter. In the CTRL run, we prescribe the total surface wind stress over the ocean using observed daily wind stress from ERA5. The model is otherwise fully interactive between the ocean and atmosphere. The CTRL run is integrated forward in time from 1 January 1941 to 31 December 2023, and the last 42 years (1982–2023) are considered in the analysis presented here. The output of CTRL is compared with observations to evaluate the model's performance.

To isolate the effects of initial conditions and wind stress anomalies on the 2023–2024 El Niño, we conducted a sensitivity experiment named InitApr2023 (Extended Data Table 2). This experiment was initialized from the CTRL hindcast on 1 April 2023, but with the 31-day running-mean wind stress anomalies removed from that date onward. The high-frequency signals within 31-day were retained to reduce model bias[36]. InitApr2023 was integrated for nine months, to 31 December 2023, thereby isolating the impact of initial conditions on 1 April 2023. Notably, 1 April 2023, was chosen as the initialization date because it coincides with the transition period of when the triple-dip La Niña had just dissipated and the 2023–2024 El Niño was about to develop. The difference between the CTRL and InitApr2023 solutions (Wind2023) represents the effects of wind stress anomalies during the El Niño event. Similarly, we conducted sensitivity experiments for the other three comparable El Niños, initialized on 1 April in the years 1982, 1997 and 2015. The composite of these experiments, referred to as InitAprOther (WindOther), indicates the impacts of initial conditions (wind stress anomalies) on other comparable El Niños. Each of these experiments was performed with three ensemble members. We limited the number of ensemble members to three because the inter-member differences in the tropical regions were found to be quite small for such wind-stress-prescribed CGCM experiments. Given that high-frequency wind stress anomalies within 31-day were

retained in both InitApr2023 and InitAprOther, which could potentially influence our conclusions, we designed two additional experiments: InitApr2023_noHighfreq and InitAprOther_noHighfreq. These experiments are identical to InitApr2023 and InitAprOther, respectively, but exclude the high-frequency wind stress anomalies within 31 days after 1 April. Supplementary Fig. 3 shows that the Niño 3 and equatorial SSTAs in the InitApr2023_noHighfreq and InitAprOther_noHighfreq experiments are nearly identical to those in the original experiments, suggesting that the synoptic-scale high-frequency wind stress anomalies have minimal impact on our main results.

We emphasize that this wind-stress-prescribed methodology provides a powerful tool for us to exactly attribute the key dynamic process underlying the 2023–2024 El Niño or other tropical climate variability. Whereas other studies have mechanically decoupled the ocean from the atmosphere by overriding wind stress in CGCMs with a simulated field[55–57], very few studies have directly used observed wind stress to drive a CGCM and then investigate the dynamic processes of observed climate variability (for example, El Niño). The successful application of this method to study the 2023–2024 El Niño indicates that this is a powerful tool for quantitatively attributing tropical climate variability and may serve as a better alternative to widely used OGCM experiments.

In addition, we performed two sets of experiments with CESM1.2.2 to evaluate the global warming effect on WPAC sea level variability. The control run, $CTRL_{CESM}$, is a pre-industrial simulation with greenhouse gas concentrations and other forcings set to 1850 levels. In this run, surface wind stress is prescribed based on values from a free-running pre-industrial simulation[47]. The $Warming_{CESM}$ run is similar to $CTRL_{CESM}$, except that the CO_2 concentration is quadrupled abruptly. It should be noted that in both experiments, the prescribed surface wind stress is identical; the only difference is the CO_2 concentration. The difference between $Warming_{CESM}$ and $CTRL_{CESM}$ could thus be used to investigate how global warming affects the sea level response to wind stress variability. Each experiment runs for 75 years, and the outputs from the last 50 years are analysed in our study. Extended Data Fig. 8h shows that compared to the present-day climate, the same wind stress variability in a future warmer climate induces stronger WPAC SLA responses, making the western Pacific region more prone to strong positive SLA events, thereby increasing the likelihood of 2023-like El Niños.

Ocean mixed layer heat budget

Here we employ a mixed layer heat budget[3,58] based on GODAS reanalysis data to investigate the detailed physical processes underlying the 2023–2024 El Niño.

$$T_t' = -(uT_x)' - (vT_y)' - (wT_z)' + \left(\frac{Q_{net} - Q_{pen}}{\rho c_p H}\right)' + R, \quad (1)$$

where T_t' indicates the temperature tendency averaged over the monthly climatological mixed layer depth (H). The first three terms on the right-hand side indicate zonal, meridional and vertical advection terms, respectively. u, v and T indicate the mixed layer averaged zonal current, meridional current and ocean temperature. w is the vertical velocity at the bottom of the mixed layer. The fourth term represents the impacts of thermal forcing. Q_{net} is the net heat flux at the ocean surface, which includes shortwave radiation, longwave radiation, latent heat flux and sensible heat flux. A positive value of Q_{net} indicates heat flux into the ocean. Q_{pen} is the solar radiation penetration at the bottom of the mixed layer depth. ρ and c_p are the density and specific heat capacity of seawater, respectively; R is the residual term. The vertical advection term $[-(\mathbf{wT_z})']$ could be further decomposed into the thermocline feedback ($-\bar{\mathbf{w}}\mathbf{T}_z'$, TH), the Ekman feedback ($-\mathbf{w}'\bar{\mathbf{T}}_z$, EK) and the nonlinear term ($-\mathbf{w}'\mathbf{T}_z'$). Here the overbar and prime denote the climatological and anomalous components, respectively.

Data availability

The OISSTv2 dataset is available at https://psl.noaa.gov/data/gridded/data.noaa.oisst.v2.highres.html; ERA5 reanalysis data at https://cds.climate.copernicus.eu/; GPCP at https://psl.noaa.gov/data/gridded/data.gpcp.html; GODAS at https://www.esrl.noaa.gov/psd/data/gridded/data.godas.html and CESM-LENS2 at https://www.cesm.ucar.edu/community-projects/lens2/data-sets.

Code availability

The code is available via Zenodo at https://doi.org/10.5281/zenodo.15074285 (ref. 59).

References

50. Reynolds, R. W., Rayner, N. A., Smith, T. M., Stokes, D. C. & Wang, W. An improved in situ and satellite SST analysis for climate. *J. Clim.* **15**, 1609–1625 (2002).
51. Adler, R. F. et al. The version-2 global precipitation climatology project (GPCP) monthly precipitation analysis (1979–present). *J. Hydrometeorol.* **4**, 1147–1167 (2003).
52. Hersbach, H. et al. The ERA5 global reanalysis. *Q. J. R. Meteorol. Soc.* **146**, 1999–2049 (2020).
53. Eyring, V. et al. Overview of the Coupled Model Intercomparison Project Phase 6 (CMIP6) experimental design and organization. *Geosci. Model Dev.* **9**, 1937–1958 (2016).
54. Delworth, T. L. et al. GFDL's CM2 global coupled climate models. Part I: formulation and simulation characteristics. *J. Clim.* **19**, 643–674 (2006).
55. Larson, S. M. & Kirtman, B. P. Revisiting ENSO coupled instability theory and SST error growth in a fully coupled model. *J. Clim.* **28**, 4724–4742 (2015).
56. Luongo, M. T., Xie, S.-P. & Eisenman, I. Buoyancy forcing dominates the cross-equatorial ocean heat transport response to Northern Hemisphere extratropical cooling. *J. Clim.* **35**, 6671–6690 (2022).
57. Larson, S. M., Buckley, M. W. & Clement, A. C. Extracting the buoyancy-driven Atlantic meridional overturning circulation. *J. Clim.* **33**, 4697–4714 (2020).
58. An, S.-I. & Jin, F.-F. Nonlinearity and asymmetry of ENSO. *J. Clim.* **17**, 2399–2412 (2004).
59. Peng, Q. Strong 2023–24 El Niño generated by ocean dynamics. *Zenodo* https://doi.org/10.5281/zenodo.15074285 (2025).

Acknowledgements

S.-P.X. was supported by the National Science Foundation (NSF, AGS 2105654) and NASA (80NSSC24M0010). A.M. was supported in part by the Japanese Ministry of Education, Culture, Sports, Science and Technology programmes for the advanced studies of climate change projection (JPMXD0722680395). M.T.L. was supported by NASA FINESST Graduate Fellowship 80NSSC22K1528 and the Cooperative Institute for Climate, Ocean, and Ecosystem Studies (CICOES) under NOAA Cooperative Agreement NA20OAR4320271, contribution number 2025-1440. The National Center for Atmospheric Research (NCAR) is sponsored by the NSF under Cooperative Agreement 1852977. We would like to acknowledge high-performance computing support from the Derecho system (https://doi.org/10.5065/qx9a-pg09) provided by the NSF NCAR, sponsored by the NSF.

Author contributions

Q.P. and S.-P.X. conceived the study. A.M., Q.P. and M.T.L. performed numerical experiments. Q.P. and A.M. conducted the analysis. Q.P. and S.-P.X. drafted the paper. Q.P., S.-P.X., A.M., C.D., P.Z. and M.T.L. contributed to interpreting the results and improving the manuscript.

Competing interests
The authors declare no competing interests.

Additional information
Extended data is available for this paper at https://doi.org/10.1038/s41561-025-01700-9.

Supplementary information The online version contains supplementary material available at https://doi.org/10.1038/s41561-025-01700-9.

Correspondence and requests for materials should be addressed to Qihua Peng or Shang-Ping Xie.

Peer review information *Nature Geoscience* thanks Michelle L'Heureux and the other, anonymous, reviewer(s) for their contribution to the peer review of this work. Primary Handling Editor: Tom Richardson, in collaboration with the *Nature Geoscience* team.

https://doi.org/10.1038/s41561-025-01700-9

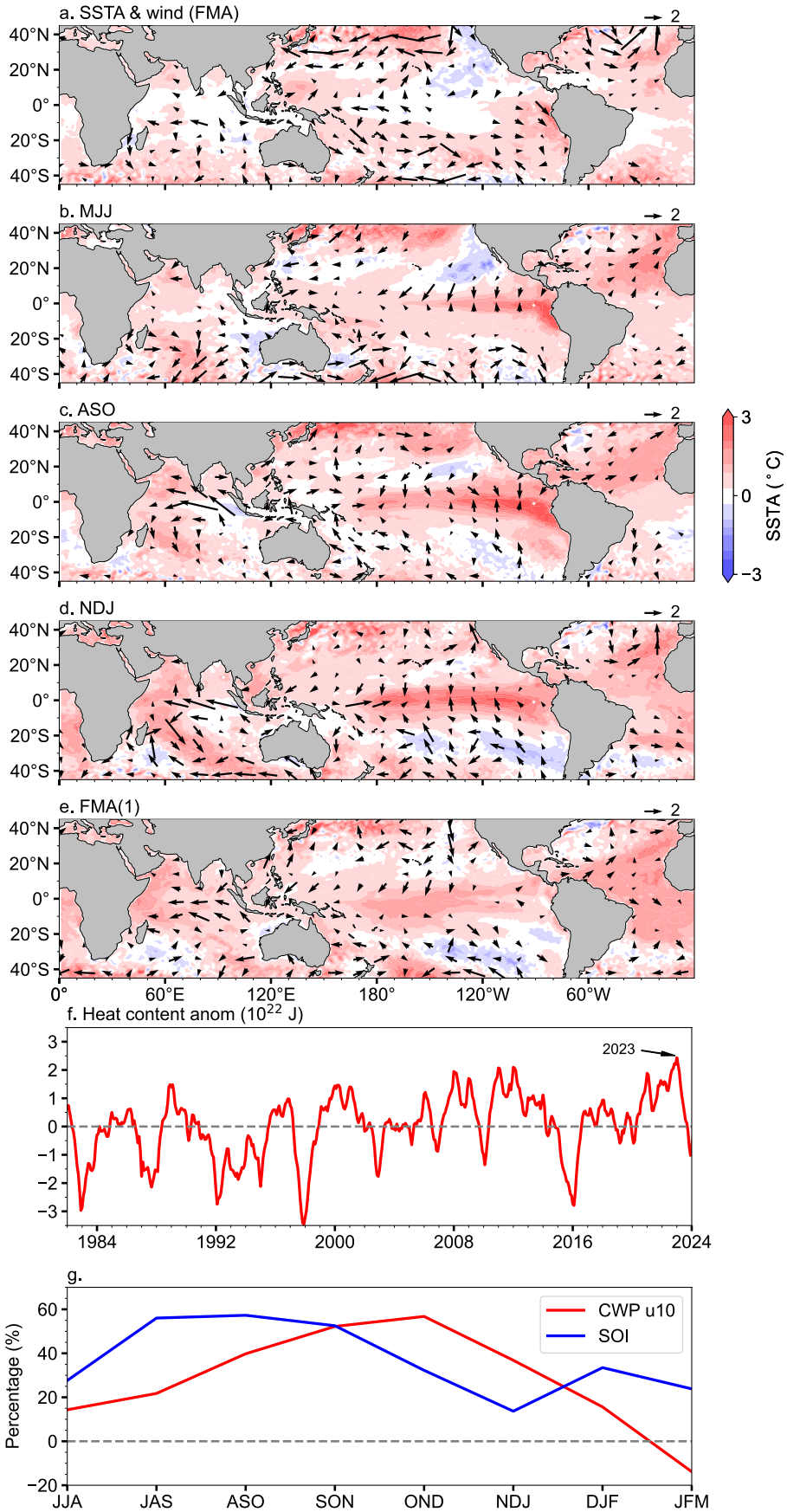

Extended Data Fig. 1 | Evolution of SSTA and 10-m wind anomalies during 2023-2024. Observed SSTA (°C, color shading) and 10-m wind anomalies (m/s, vectors) averaged in (**a**) February-April (FMA), (**b**) May-July (MJJ), (**c**) August-October (ASO), (**d**) November-January (1) (NDJ), and (**e**) FMA 2024. Time series of (**f**) upper-300 m OHC anomalies (10^{22}J) in the western Pacific Ocean (WPAC, 130°E–180°, 10°S–10°N) and (**g**) percentage of 2023–2024 observed CWP u10 and SOI compared to their expected values derived from regression analysis. All anomalies are defined relative to the period 1982-2022.

https://doi.org/10.1038/s41561-025-01700-9

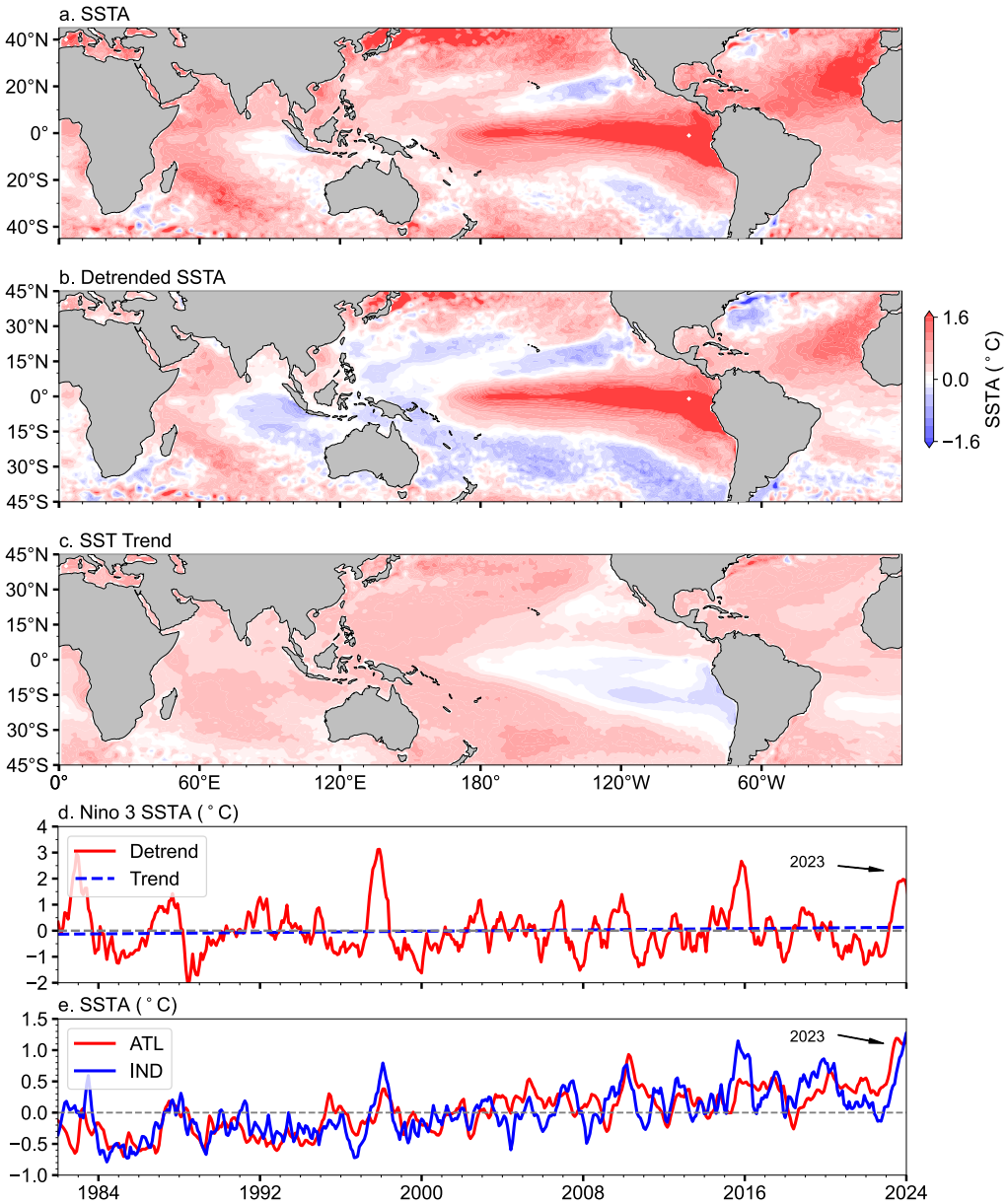

Extended Data Fig. 2 | Decomposition of observed SSTA for the AGCM experiments. The June-December 2023 averaged (**a**) SSTA (°C), (**b**) detrended SSTA component, and (**c**) the background SST trend component for the period 1982-2023, obtained by subtracting (**b**) from (**a**). All anomalies are calculated with reference to the 1982–2022 climatological values. Time series of (**d**) detrended and trended Niño3 index as well as (**e**) SSTAs averaged over the tropical North Atlantic (0-70°W, equator-30°N) and tropical western Indian Ocean (40°E-70°E, 10°S-10°N).

https://doi.org/10.1038/s41561-025-01700-9

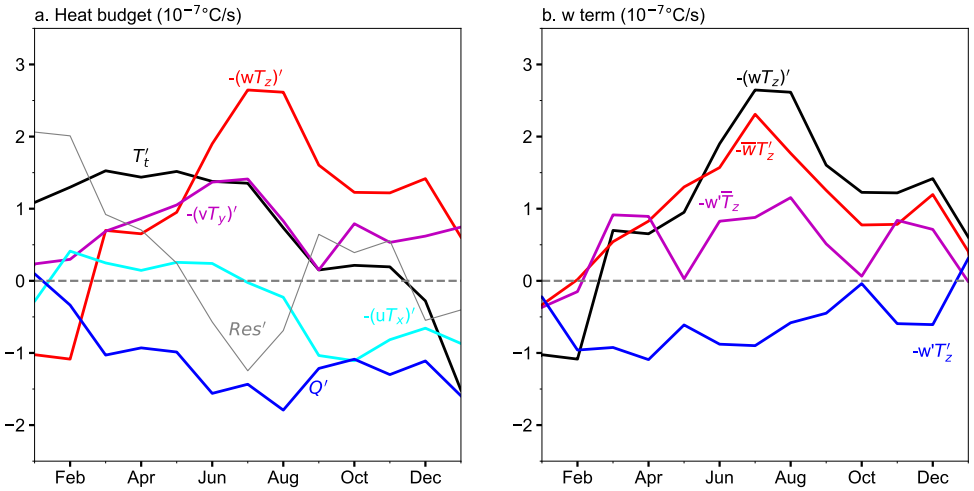

Extended Data Fig. 3 | The mixed layer heat budget for the 2023-2024 El Niño. (**a**) Heat budget terms of the 2023-2024 El Niño (10^{-7}°C/s, averaged in Niño 3 region) (see Materials and Methods). (**b**) The relative importance of thermocline feedback (TH, red line), Ekman feedback (EK, magenta line), and the nonlinear term (blue line) in modulating the vertical advection term. These results are derived from reanalysis data.

https://doi.org/10.1038/s41561-025-01700-9

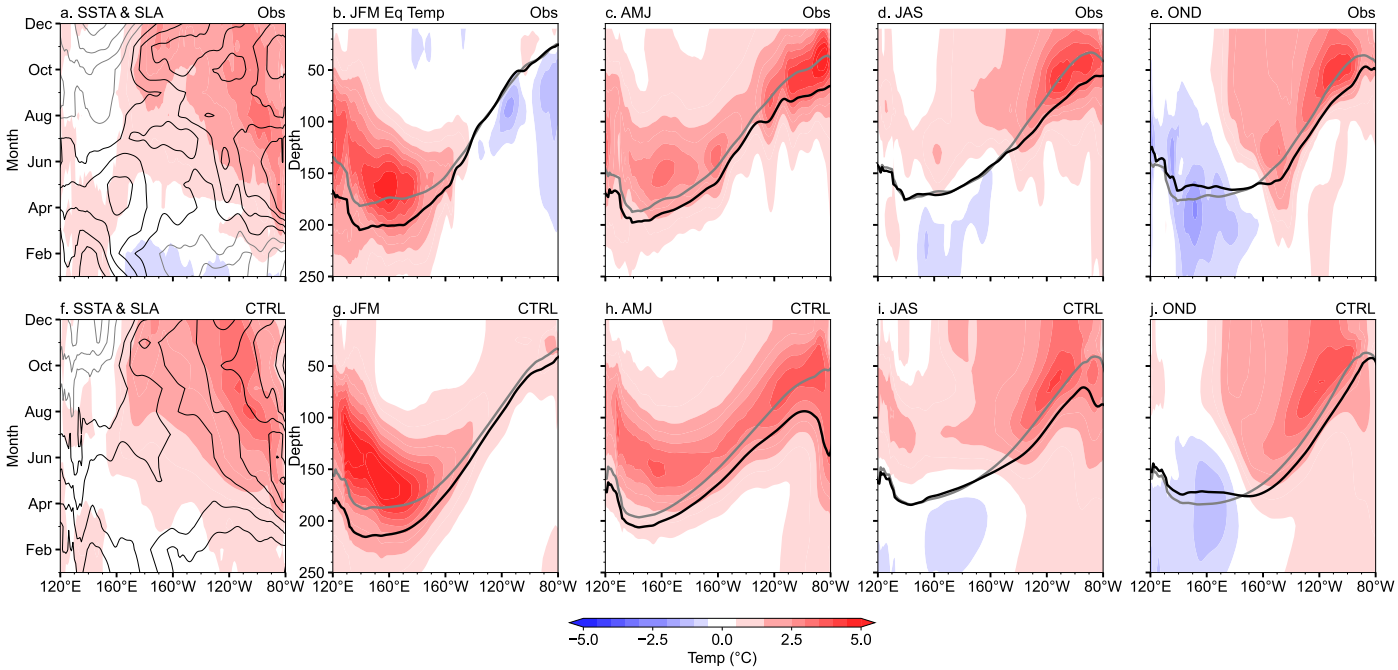

Extended Data Fig. 4 | Comparison of the observed and simulated ocean temperature anomalies for the 2023-2024 event. (**a**) Longitude-time diagram of observed equatorial SSTAs (color shading; °C) and SLAs (contours with an interval of 3 cm; positive black and negative gray). (**b**)-(**e**) shows the evolution of observed equatorial ocean temperature anomalies (°C, color shading) for the 2023-2024 El Niño averaged over (**a**) January-March (JFM), (**b**) April-June (AMJ), (**c**) July-September (JAS), and (**d**) October-December (OND). (**f**)-(**j**) Similar to the upper panels but from the CTRL run. The black (grey) line represents the 2023 (climatological) 20 °C isotherm. All meridionally averaged over 2°S–2°N.

https://doi.org/10.1038/s41561-025-01700-9

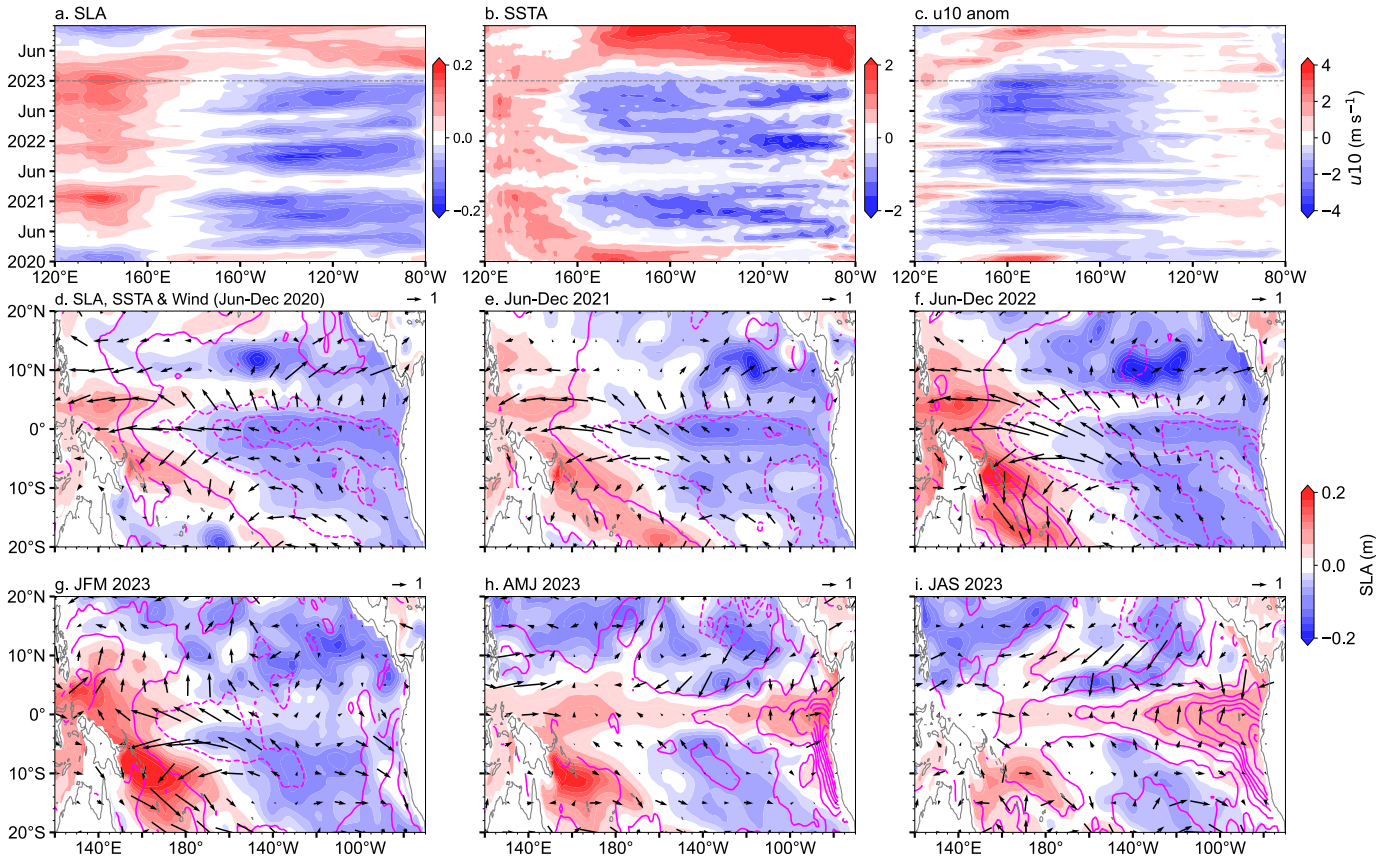

Extended Data Fig. 5 | Observed climate state during 2020-2023. Longitude-time evolution of the (**a**) equatorial SLA (m), (**b**) SSTA (°C), and (**c**) 10-m zonal wind anomalies (m/s) during January 2020-December 2023. All meridionally averaged over 2°S–2°N. (**d**)-(**f**) Observed SLA (m, color shading), SSTA (contours with a 0.2 °C interval), and surface wind anomalies (m/s, vectors) averaged over June–December for the years 2020, 2021, and 2022, respectively. The lower panels are similar to the middle panels but averaged in (**g**) JFM, (**h**) AMJ, and (**i**) JAS 2023, respectively.

https://doi.org/10.1038/s41561-025-01700-9

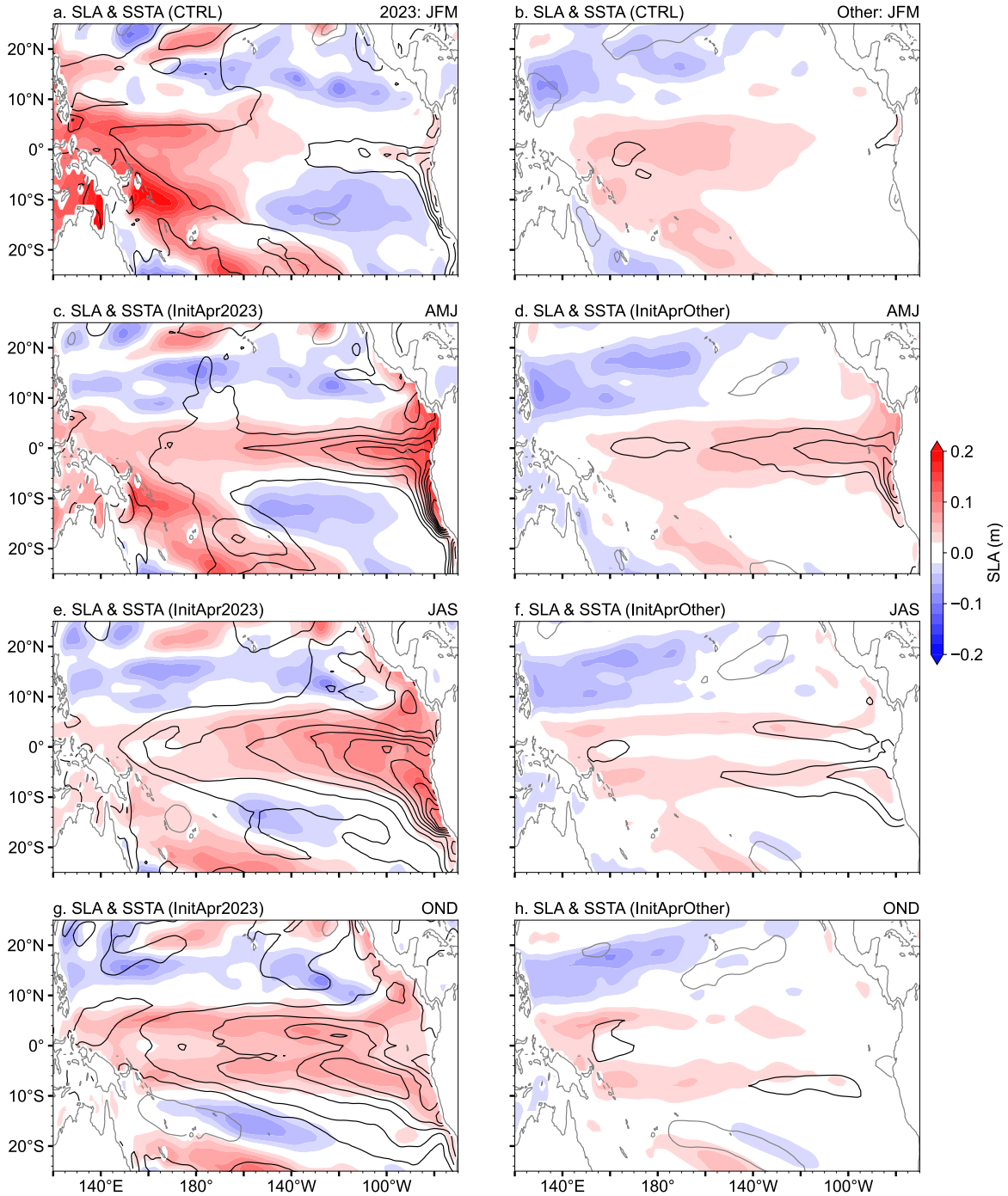

Extended Data Fig. 6 | The impacts of initial condition on the 2023-2024 and other comparable El Niños. Simulated SLA (m, color shading) and SSTA (contours with an interval of 0.5 °C; positive black and negative gray) in (**a**) January-March (JFM) 2023 from the CTRL Run, which roughly describes the initial condition for the InitApr2023. (**c**), (**e**), and (**g**) same as (**a**) but averaged in (**c**) AMJ, (**e**) JAS, and (**g**) OND from the InitApr2023 experiment. The right panels are similar to the left panels but for other comparable El Niño composites.

https://doi.org/10.1038/s41561-025-01700-9

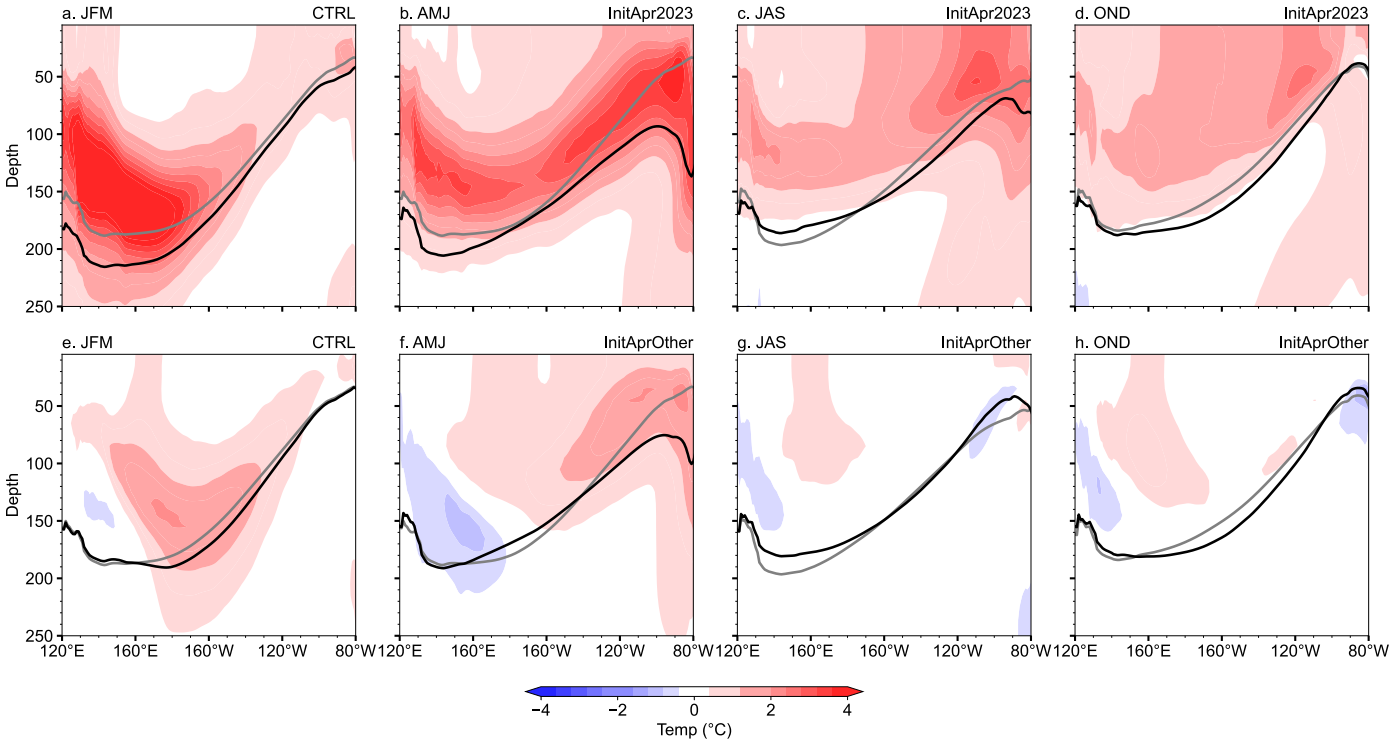

Extended Data Fig. 7 | Equatorial temperature changes from the InitApr2023 and InitAprOther experiments. (**a**) The JFM ocean temperature anomalies from the CTRL run, which generally describes the initial condition for the InitApr2023. (**b**)-(**d**) The evolutions of equatorial ocean temperature anomalies averaged over (**a**) JFM, (**b**) AMJ, (**c**) JAS, and (**d**) OND from InitApr2023. (**e**)-(**h**) Similar to upper panels but for the other comparable El Niño composite (InitAprOther). The black (grey) line represents the 2023 (climatological) 20 °C isotherm. All panels are meridionally averaged over 2°S–2°N.

https://doi.org/10.1038/s41561-025-01700-9

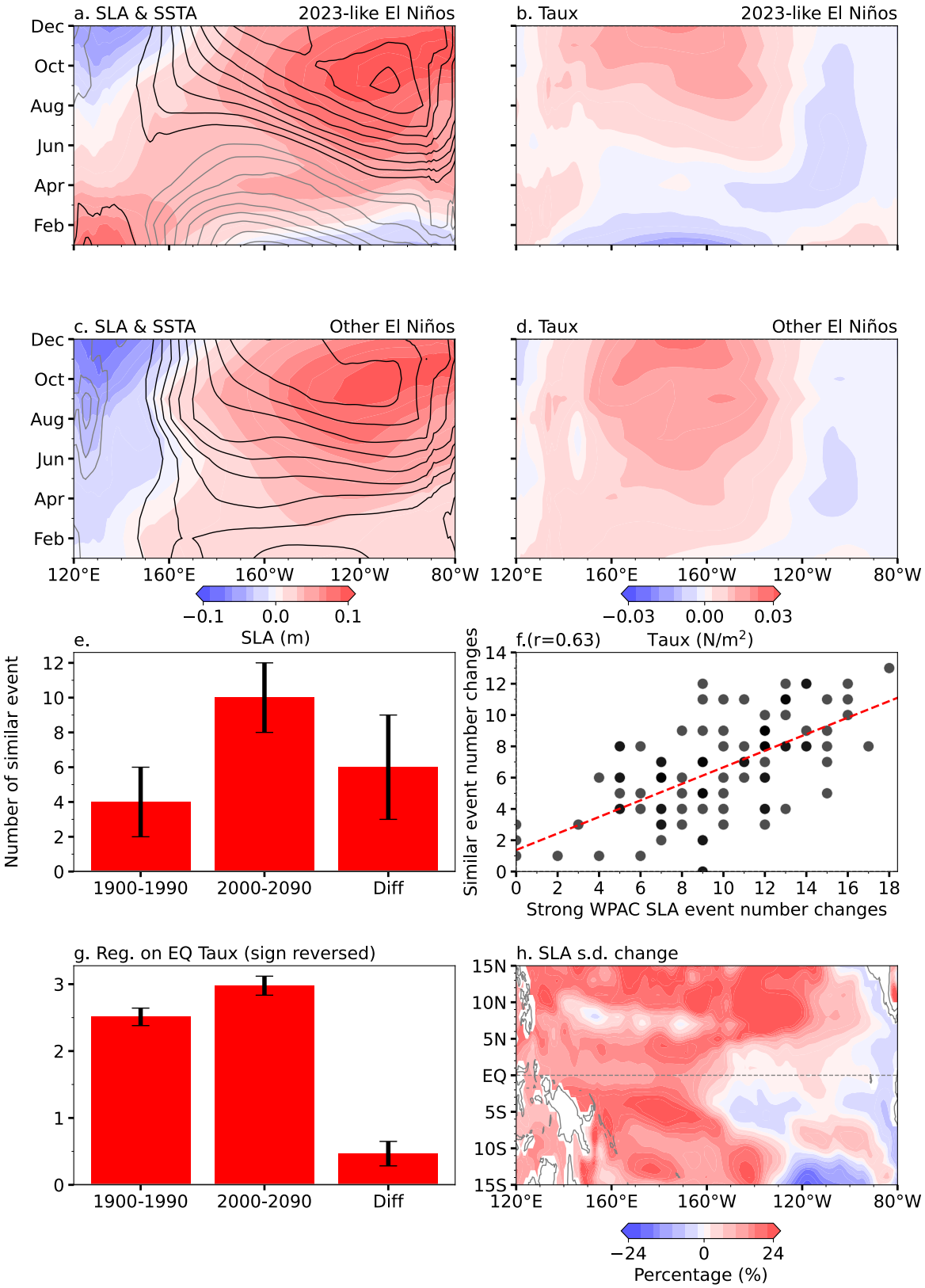

Extended Data Fig. 8 | See next page for caption.

https://doi.org/10.1038/s41561-025-01700-9

Extended Data Fig. 8 | Future changes in 2023-like El Niños. Hovmöller diagram of equatorial (**a**) SLA (m, color shading) and SSTA (°C, contours with an interval of 0.2 °C; positive black and negative gray), and (**b**) zonal wind stress (color shading; N/m^2) for the 2023-like El Niño composites during 1900-1990. (**c**)-(**d**) Same as (**a**)-(**b**) but for other non-2023-like El Niños. (**e**) Comparison of the ensemble mean (bars) number of 2023-like El Niño (see Materials and Methods) during 1900-1990 and 2000-2090, along with their differences. The error bars indicate inter-member ±1 standard deviation (n = 99). (**f**) Scatter plot for changes in the number of strong positive SLA events in the WPAC region during JFM (SLA > 4.5 cm) and changes in the number of 2023-like El Niño events. (**g**) Regression (sign reversed) of WPAC JFM SLA (m) onto the preceding August (−1)-January equatorial (averaged over 130°E–90°W and 2°S–2°N) zonal wind stress anomalies (Taux) during 1900–1990 and 2000–2090, along with their differences. Bars (errorbars) are the ensemble mean (inter-member ±1 standard deviation) (n = 99). (**a**)-(**g**) are derived from the CESM-LENS2 simulations. (**h**) Simulated JFM interannual SLA s.d. percentage changes due to global warming, calculated as the difference between the $Warming_{CESM}$ and $CTRL_{CESM}$ experiments (see Methods).

https://doi.org/10.1038/s41561-025-01700-9

Extended Data Table 1 | Description of the AGCM experiments

Experiments	Forcings	Description
aCTRL	Climatological SST+2023 SSTA	All 2023 SSTA included
aPac	Climatological SST+2023 Pacific detrended SSTA	Impacts of 2023 Pacific detrended SSTA
aIndAtl	Climatological SST+2023 Indian-Atlantic detrended SSTA	Impacts of Indian-Atlantic detrended SSTA
aTrend	Climatological SST+ Global SST trend	Impacts of global SST trend
aPac_RSST	Climatological SST+2023 Pacific relative SSTA	Impacts of 2023 Pacific relative SSTA

https://doi.org/10.1038/s41561-025-01700-9

Extended Data Table 2 | Summary of the wind stress-prescribed CGCM experiments

Experiments	Wind stress	Description
CTRL	Daily ERA5 wind stress during 1941-2023.	All processes included
InitApr2023	Initialized on 1 April 2023. 31-day running-mean wind stress anomalies are removed after 1 April 2023. High-frequency wind stress anomalies within 31-day are retained.	Impacts of initial conditions on the 2023-24 El Niño
Wind2023	-	Derived as the difference, CTRL-InitApr2023. The result indicates the impacts of wind stress anomalies in 2023
InitAprOther	Same as InitApr2023, but 31-day running-mean wind stress anomalies are removed after Apr 1 in other comparable El Niños of 1982/83, 1997/98, and 2015/16. High-frequency wind stress anomalies within 31-day are retained.	Impacts of initial conditions on the other comparable El Niño events
WindOther	-	Derived as the difference, CTRL-InitAprOther. The result indicates the impacts of wind stress anomalies in the other comparable El Niño events
InitApr2023_noHighfreq	Same as InitApr2023, but high-frequency wind stress anomalies within 31-day are removed.	Evaluate the effect of high-frequency wind stress within 31 days on the 2023-24 El Niño by comparing the results with those from InitApr2023
InitAprOther_noHighfreq	Same as InitAprOther, but high-frequency wind stress anomalies within 31-day are removed.	Assess the impacts of high-frequency wind stress within 31 days on the other comparable El Niño events by comparing the results with those from InitAprOther